

# A Reversible and Visible Colorimetric/Fluorescent Chemosensor for $\text{Al}^{3+}$ and $\text{F}^-$ ions with a Large Stoke's Shift

Yuan-Hui Zhao<sup>a</sup>, Xi Zeng<sup>a</sup>, Lan Mu<sup>a,\*</sup>, Jun Li<sup>a</sup>, Carl Redshaw<sup>b</sup> and Gang Wei<sup>c,\*</sup>

<sup>a</sup> Key Laboratory of Macrocyclic and Supramolecular Chemistry of Guizhou Province, Guizhou University, Guiyang 550025, P.R. China

<sup>b</sup> Department of Chemistry, University of Hull, Hull HU6 7RX, U.K.

<sup>c</sup> CSIRO Materials Science and Engineering, P. O. Box 218, Lindfield, NSW 2070, Australia

**ABSTRACT:** A novel quinoline-vinyl-dihydroxyphenyl linkage with donor- $\pi$ -bridge-acceptor structural motif, where quinoline serves as an electron-withdrawing core has been synthesized and used as a fluorescent sensor (**2**) for recognition of  $\text{Al}^{3+}$  and  $\text{F}^-$  by colorimetric/fluorescent. The sensor **2** shows almost no fluorescence due to excited-state intramolecular proton transfer (ESIPT) from the hydroxyl oxygens to the nitrogen of quinoline moiety. Coordination of  $\text{Al}^{3+}$  or  $\text{F}^-$  with sensor **2** creates strong fluorescence at 545 nm or 575 nm, respectively, due to the suppression of ESIPT and reducing of intramolecular charge transfer (ICT). A reversible “off-on-” optical switch mode has been constituted by sequential inputs  $\text{Al}^{3+}$  and  $\text{F}^-$  ions to the sensor **2** with different excitation and emission wavelengths.  $^1\text{H}$  NMR and IR analysis revealed that the  $\text{Al}^{3+}$  is coordinated with quinoline nitrogen atoms and phenolic oxygen atoms, however, the  $\text{F}^-$  center is only coordinated with two phenolic oxygen atoms. The difference structure of **2**- $\text{Al}^{3+}$  and **2**- $\text{F}^-$  complexes result in different-wavelength fluorescence.  $^1\text{H}$  NMR revealed that  $\pi$  electrons on the excited state of sensor and ion complexes are delocalized over the molecules. This different electron density results in different wavelength fluorescence.

**Keywords:** Quinaldine, ESIPT, ICT, Fluorescent/colorimetric sensor,  $\text{Al}^{3+}$ ,  $\text{F}^-$

## Introduction

Both cations and anions are ubiquitous and play critical roles in many biological, chemical and environmental systems. Not only the scientific community, especially chemists, biologists, and environmentalists, but also the increasingly general population all concerned about them because of the environmental and health

problems [1-2]. Aluminum is found in most animal and plant tissues as well as in natural waters. The soluble form of it often endangers the aquatic life and influences agricultural production [3-4]. Due to its widespread use [5], a significant load of aluminum ions exceeds the human body's excretory capacity; the excess is deposited in various tissues. The unregulated amounts of aluminum in brain may lead to the malfunction of central nervous system [6-7].

Moreover, among the biologically important anions, fluoride is of particular interest owing to its role in preventing dental caries, and in the treatment for osteoporosis. It is a common ingredient in drugs and cockroach poisons [8]. Excess fluoride ion exposure causes fluorosis, thyroid activity depression, bone disorders and immune system disruption [9-11].

The fluorescent sensing method has been developed as a useful tool for detecting ions due to the simplicity, high sensitivity, high selectivity, and real-time detection [12-13]. Although a number of  $F^-$  [14-17] and  $Al^{3+}$  ion [18-21] fluorescent sensors have been reported, but exhibit obvious fluorescence response to both  $F^-$  and  $Al^{3+}$  are rather rare. Most of the dual functional fluorescent sensors for anions and cations are based on the displacement approach [22-23], which means the sensing output mode is single and the selectivity may be limited. In addition, the detection of  $Al^{3+}$  has always been problematic due to the lack of spectroscopic characteristics and poor coordination ability compared to transition metals [24]. In order to develop new multifunctional fluorescent sensors and improve the sensing properties, the design of the sensors for selectively detection of  $F^-$  and  $Al^{3+}$  with new sensing mechanism is still a quite important and intriguing theme. 8-Hydroxy quinoline (8-HQ) core is an efficient candidate for metal ion recognition and widely used for the synthesis of chemosensors for selective detection of alkali, alkaline earth and transition metal ions [25-28]. It has been shown that the photophysical properties of 8-HQ can be easily manipulated by virtue of the nature of substituents at the 8-position to behave either as a fluorescence "on-off" or "off-on" sensor [29]. There also have been reports on modifications of 8-HQ core at the aromatic ring at 2- or 6 and 7-position by bringing additional binding sites to form extending  $\pi$ -system which can act as fluorescent

sensor with large Stoke's shift(>100nm) [30-31].

Herein, we report on the synthesis of a novel 2-styrylquinoline based sensor **2** with donor- $\pi$ -bridge-acceptor (D- $\pi$ -A) structural motif through a simple condensation. The sensor has a fully conjugated fluorophore structure with both metal and anion ions receptor. Thus, it can high selectivity and sensitivity to proper binding with  $Al^{3+}$  or  $F^-$  through the intramolecular charge transfer (ICT) mechanism with an intrinsic large Stoke's shift (>100 nm). It also can use as "nake eye" detection and reversible molecular switcher.

## 2. Experimental

### 2.1. Materials and equipments

The solutions of metal ions were prepared from their nitrate salts (Aldrich and Alfa Aesar Chemical Co., Ltd.). All the anions are tetra-n-butylammonium salts (Sigma-Aldrich Chemical Co.), stored in a desiccator under vacuum containing self-indicating silica, and used without any further purification. Other chemicals used in this work were of analytical grade and used without further purification. Double distilled water was used.

Fluorescence spectroscopy measurements were performed on a Cary Eclipse fluorescence spectrophotometer (Varian) equipped with a xenon discharge lamp using a 1 cm quartz cell. UV-vis spectra were recorded on a UV-1800 spectrophotometer (Beijing General Instrument Co., China). IR spectra were obtained using a Vertex 70 FT-IR spectrometer (Bruker). Melting points were determined on an X-5 binocular microscope (Beijing Tech Instrument Co., China).  $^1H$  and  $^{13}C$  NMR spectra were measured with Nova-400 NMR spectrometers (Varian) and WNMR-I 500MHz NMR (Wuhan Institute of Physics and Mathematics, Chinese Academy of Sciences) at room temperature using TMS as an internal standard. ESI-MS spectra were recorded on a HPLC-MSD-Trap-VL spectrometer (Agilent). Isothermal titration calorimetry (ITC) experiments were performed using an isothermal titration calorimeter a Nano ITC (TA); All experiments were carried out at room temperature (~ 298K).

## 2.2. Solution preparation

The sensor **2** stock solution ( $1.00 \times 10^{-4}$  M) was prepared in a 100 mL volumetric flask, with 2.8 mg of sensor **2** was dissolved in  $\text{CH}_3\text{CN}$  and then diluting to the mark.

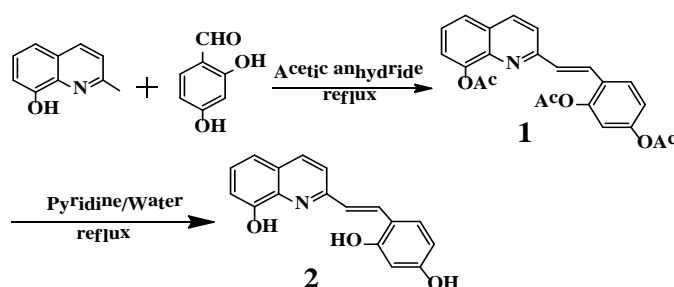
$\text{Al}^{3+}$  stock solution ( $2.00 \times 10^{-3}$  M) were prepared in a 50 mL volumetric flask by dissolving 40.0 mg  $\text{Al}(\text{NO}_3)_3$  in  $\text{H}_2\text{O}$ , and then diluting to the mark with  $\text{H}_2\text{O}$ . The other metal ions were prepared as ( $2.00 \times 10^{-3}$  M) water solutions; anions were prepared as ( $2.00 \times 10^{-3}$  M)  $\text{CH}_3\text{CN}$  solutions. Tris-HCl buffer stock solution was prepared in acetonitrile ( $1.00 \times 10^{-3}$  M, pH 7) with the proper amount of HCl.

$\text{F}^-$  stock solution ( $2.00 \times 10^{-3}$  M) was prepared in a 100 mL by dissolving 63.1 mg tetra-*n*-butylammonium acetate in  $\text{CH}_3\text{CN}$  and then diluting to the mark. The  $^1\text{H}$  NMR experiment used analytical grade  $\text{Al}(\text{ClO}_4)_3$ .

ITC experiment consisted of 16 consecutive injections ( $10 \mu\text{L}$ ) of ion solution ( $\text{Al}^{3+}$ ,  $\text{F}^-$ ,  $1 \times 10^{-3}$  M) into the microcalorimetric reaction cell (1 mL) charged with a solution of sensor **2** ( $5 \times 10^{-5}$  M). The heat of reaction was corrected for the heat of dilution of the ion solution determined in the separate experiments. All solutions were degassed prior to titration experiment by sonication. Computer simulations (curve fitting) were performed using the Nano ITC analyze software.

## 2.3. Synthesis of sensors

The intermediate (derivative **1**) was synthesized from 8-hydroxyquinoline and 2,4-dihydroxybenzaldehyde in acetic anhydride solvent, and then further hydrolyzed in pyridine/water mixed solvent to give sensor **2** {(E)-8-hydroxyl-2-[(E)-2-(2,4-dihydroxy phenyl)vinyl]-quinoline}. The synthetic route was carried out as outlined in Scheme 1:



**Scheme 1** Synthesis of quinoline derivative **1** and sensor **2**

### 2.3.1 Synthesis of sensor **2**

To a solution of 8-hydroxyquinaldine (1.00 g, 6.29 mM) in acetic anhydride (10 mL) was added 2,4-dihydroxybenzaldehyde (0.87 g, 6.29 mM). The mixture was heated under reflux for 5 h. Enrichment to remove solvent acetic anhydride, the crude product was purified with column chromatography over silica gel using chloroform/ethyl acetate (3/1, v/v) as the eluent to get the desired compound in pure form. Yield an intermediate (sensor **1**) as a white solid (1.78 g, 70 %).

A solution of sensor **2** (0.81 g, 2.00 mM in pyridine, 15 mL) was refluxed for 30 min, and water (5 mL) was added. The reaction mixture was refluxed for 11 h. After the mixture was cooled, water (100 mL) was added to the mixture, extracted with n-butyl alcohol (50mL×3), organic layer was washed with distilled water (30mL×2), then was washed with saturated salt water 30 mL, n-butyl alcohol layer was dried with anhydrous sodium sulfate overnight. The organic layer was separated and the solvents were evaporated. The residue eluted from a column chromatography of silica gel with chloroform/methanol (9/1, v/v) to give the red brown desired product sensor **2** (0.50 g, 89.0%). m.p. 195~197°C; <sup>1</sup>H NMR (DMSO-*d*<sub>6</sub>, 400 MHz) δ (ppm): 6.29 (d, J=8.56 Hz, 1H, Ar-H), 6.37 (s, 1H, Ar-H), 7.02~7.03 (m, 1H, Ar-H), 7.28~7.31 (m, 3H, Ar-H), 7.41 (d, J=8.24 Hz, 1H, Ar-H), 7.70 (d, J=8.52 Hz, 1H, C=CH), 7.96 (d, J=16.56 Hz, 1H, Ar-H), 8.18 (d, J=8.64 Hz, 1H, C=CH), 9.43 (s, 1H, OH), 9.62 (s, 1H, OH), 9.87 (s, 1H, OH). <sup>13</sup>C NMR (CDCl<sub>3</sub>, 400 MHz) δ (ppm): 160.5, 158.3, 156.8, 153.7, 139.4, 137.4, 131.2, 129.5, 128.9, 127.5, 125.7, 120.6, 118.8, 116.9, 111.8, 108.7, 103.5. ESI-MS *m/z*: 280.1 ([M+H]<sup>+</sup>), calcd. for C<sub>17</sub>H<sub>13</sub>NO<sub>3</sub>= 279.321. IR (KBr, cm<sup>-1</sup>) *v*: 3233, 3052, 1590, 1522, 1495, 1440, 1387, 1235, 1193, 1096, 975, 867, 747, 449. (Fig. S1-S4).

### 3. Results and discussion

#### 3.1 Spectral studies

##### 3.1.1 Fluorescence spectral for metal ions

The sensor **2** exhibited weak fluorescence in CH<sub>3</sub>CN/H<sub>2</sub>O (5/2, v/v, Tris-HCl buffer, pH 7) solution due to the excited-state intramolecular proton transfer (ESIPT) from oxygen to nitrogen. Addition of Al<sup>3+</sup> ion results in an obviously enhanced fluorescence at 545 nm, the fluorescent intensity was remarkably enhanced (26-fold),

showing the “off-on” fluorescence emission, while other ions induce much smaller or no fluorescence increases, as shown in Fig. 1A. First, the fluorescence could increase dramatically attributed to the main quenching process (ESIPT) is suppressed and causes an enhancement in the emission. Second, coordination of the  $\text{Al}^{3+}$  to the ligand that is conjugated to the quinoline core suppressed the ICT process also contributes to the fluorescence intensity enhancement. At the same time lead to the emission wavelength red shift and a clear green fluorescence could be observed under ultraviolet light (Fig. 1A, inset). These changes stopped and the emission intensities became constant when the amount of  $\text{Al}^{3+}$  added reached 1 equiv (Fig. 1B). Job plot analysis of the fluorescence titrations revealed 1:1 binding stoichiometry (Fig. 1B, inset). The association constant for  $\text{Al}^{3+}$  was estimated to be  $1.52 \times 10^4 \text{ M}^{-1}$  by using Stern-Volmer plot assuming 1:1 stoichiometry (Fig. S5). Whereas competitive metal ions displayed much weaker response, and the coexisting metal ions did not interfere with the detection of  $\text{Al}^{3+}$  (Fig. S6).

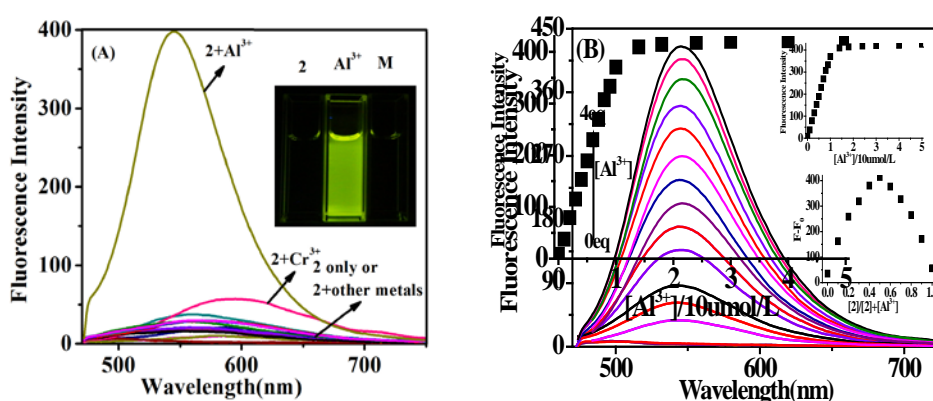


Fig. 1. Fluorescence spectra of sensor **2** ( $10 \mu\text{M}$ ,  $\text{CH}_3\text{CN}/\text{H}_2\text{O}$ , v/v, 5/2, pH 7) with different metal ions (A), inset shows the color change of sensor **2** in the absence and the presence of  $\text{Al}^{3+}$  under UV light. The spectra titrations of sensor **2** with  $\text{Al}^{3+}$  (B), inset shows variation of fluorescence intensity against the number of equivalents of  $\text{Al}^{3+}$  and Job's plot data. Metal ions ( $200 \mu\text{M}$ ) including  $\text{Li}^+$ ,  $\text{Na}^+$ ,  $\text{K}^+$ ,  $\text{Mg}^{2+}$ ,  $\text{Ca}^{2+}$ ,  $\text{Ba}^{2+}$ ,  $\text{Sr}^{2+}$ ,  $\text{Hg}^{2+}$ ,  $\text{Pb}^{2+}$ ,  $\text{Cd}^{2+}$ ,  $\text{Zn}^{2+}$ ,  $\text{Co}^{2+}$ ,  $\text{Ni}^{2+}$ ,  $\text{Cu}^{2+}$ ,  $\text{Ag}^+$ ,  $\text{Cr}^{3+}$ ,  $\text{Fe}^{3+}$ .  $\lambda_{\text{ex}}/\lambda_{\text{em}} = 440/545 \text{ nm}$

### 3.1.2 Absorption spectra for metal ions

Upon addition of various above-mentioned ions ( $200 \mu\text{M}$ ) to sensor **2** ( $10 \mu\text{M}$ ,  $\text{CH}_3\text{CN}/\text{H}_2\text{O}$ , 5/2, v/v, Tris-HCl, pH 7) solution, a strong absorption band was observed only in the presence of  $\text{Al}^{3+}$  ion with a concomitant decrease at 360 nm, the

maximum absorption peak moves to 430nm (redshift about 70 nm), other ions lead to almost no spectral changes (Fig. 2A). The absorbance ratio ( $A_{430}/A_{360}$ ) showed clear sigmoid dependence on the  $Al^{3+}$  concentration (Fig. S7), and the ratiometric absorbance change could be potentially useful for quantitative determination of  $Al^{3+}$ . Meanwhile the color changed to bright yellow, which could be observed by the naked eye (Fig. 2A, inset). With the increase of the concentration of  $Al^{3+}$ , three clear isosbestic points were observed at 260 nm, 280 nm and 385 nm, respectively (Fig. 2B). Indicating that there was balance between the complex, sensor, and ion in solution. When the amount of  $Al^{3+}$  was greater than 1 equiv sensor **2**, the absorbance reached saturation. The stoichiometry of the interaction reveals that a 1:1 between sensor **2** and  $Al^{3+}$ , and also supported by Job's plot data (Fig. 2B, inset). On the basis of the absorption of sensor **2** as a function of  $Al^{3+}$  concentration, the association constant for sensor **2** with  $Al^{3+}$  was calculated to be  $1.4 \times 10^4 M^{-1}$  using Stern-Volmer plot (Fig. S8). The response of sensor **2** for metal ion and the effect of coexisting ions to  $2-Al^{3+}$  had shown that the other competition metal ions did not interfere with the detection of  $Al^{3+}$  (Fig. S9).

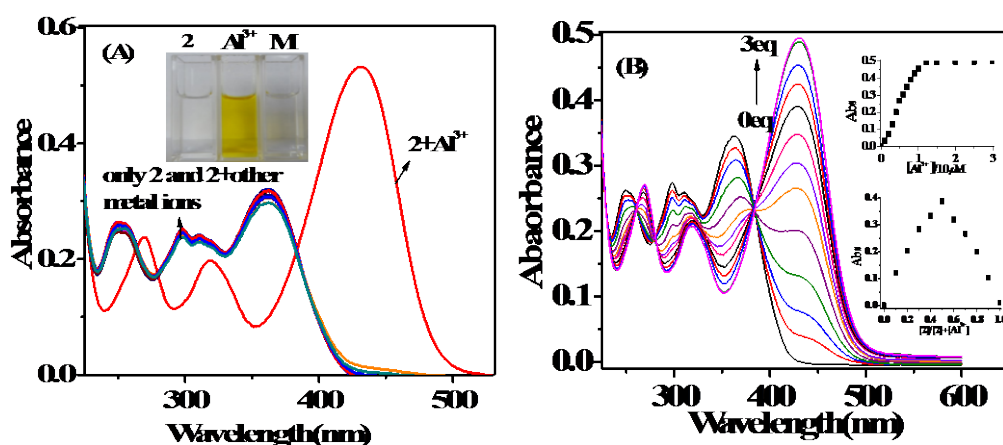


Fig. 2. Absorption spectra of sensor **2** ( $10 \mu M$ ,  $CH_3CN/H_2O$ , 5/2, v/v, pH 7) with different metal ions (A), inset shows the color change of sensor **2** in the absence and the presence of  $Al^{3+}$  under visible light. The spectra titrations of **2** with  $Al^{3+}$  (B). Metal ions ( $200 \mu M$ ) including  $Li^+$ ,  $Na^+$ ,  $K^+$ ,  $Mg^{2+}$ ,  $Ca^{2+}$ ,  $Ba^{2+}$ ,  $Sr^{2+}$ ,  $Hg^{2+}$ ,  $Pb^{2+}$ ,  $Cd^{2+}$ ,  $Zn^{2+}$ ,  $Co^{2+}$ ,  $Ni^{2+}$ ,  $Cu^{2+}$ ,  $Ag^+$ ,  $Cr^{3+}$ ,  $Fe^{3+}$ .  $\lambda_{max} = 430 \text{ nm}$

### 3.1.3 Spectral characteristics of sensor **2** for anions

Under excitation at 465 nm, in the absence and in the presence of anions ( $Cl^-$ ,  $Br^-$ ,  $I^-$ ,

NO<sub>3</sub><sup>-</sup>, AcO<sup>-</sup>, H<sub>2</sub>PO<sub>4</sub><sup>-</sup>, PF<sub>6</sub><sup>-</sup>, ClO<sub>4</sub><sup>-</sup>, HSO<sub>4</sub><sup>-</sup>) the fluorescence spectrum of sensor **2** did not reveal any significant changes except for F<sup>-</sup>. Addition of F<sup>-</sup> ion results in an obviously enhanced fluorescence at 575 nm, showing the “off-on” fluorescence emission (Fig. 3A) and a yellow fluorescence could be observed under ultraviolet light (Fig. 3A, inset). This observation was consistent with the fact that the F<sup>-</sup> interacted with protons of phenolic hydroxyl through hydrogen-binding. When 20 equiv. of F<sup>-</sup> was added, the fluorescence enhancement factor was 24-fold approximately. The emission intensities became constant when the amount of F<sup>-</sup> added reached 1 equiv. (Fig. 3B). Job plot analysis of the fluorescence titrations revealed 1:1 binding stoichiometry (Fig. 3B, inset), and the association constant for F<sup>-</sup> was estimated to be 4.1×10<sup>4</sup> M<sup>-1</sup> (Fig. S10). Whereas above mentioned competitive anions displayed much weaker response, and did not interfere the ability of sensor **2** detection of F<sup>-</sup> (Fig. S11).

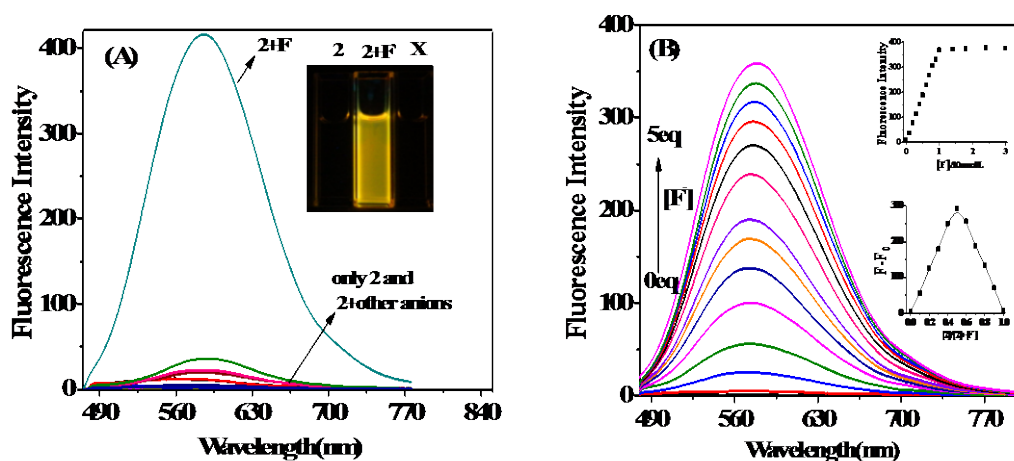


Fig. 3. Fluorescence spectra of sensor **2** (10 μM, CH<sub>3</sub>CN) with different anions (A), inset shows the color change of sensor **2** in the absence and the presence of F<sup>-</sup> under UV light. Fluorescence spectra titrations of sensor **2** with F<sup>-</sup> (B), inset shows variation of fluorescence intensity against the number of equivalents of F<sup>-</sup> and Job's plot data. Anions (200 μM) include Cl<sup>-</sup>, Br<sup>-</sup>, I<sup>-</sup>, NO<sub>3</sub><sup>-</sup>, AcO<sup>-</sup>, H<sub>2</sub>PO<sub>4</sub><sup>-</sup>, PF<sub>6</sub><sup>-</sup>, ClO<sub>4</sub><sup>-</sup>, HSO<sub>4</sub><sup>-</sup>. λ<sub>ex</sub>/λ<sub>em</sub>=465/575 nm.

In the absence of the anion (F<sup>-</sup>, Cl<sup>-</sup>, Br<sup>-</sup>, I<sup>-</sup>, NO<sub>3</sub><sup>-</sup>, AcO<sup>-</sup>, H<sub>2</sub>PO<sub>4</sub><sup>-</sup>, PF<sub>6</sub><sup>-</sup>, ClO<sub>4</sub><sup>-</sup>, HSO<sub>4</sub><sup>-</sup>), sensor **2** has an absorption maximum at 360 nm, which can be assigned to conjugate absorption band of molecular. With the addition of the anion (200 μM) to a

solution of sensor **2** ( $10\ \mu\text{M}$ ,  $\text{CH}_3\text{CN}$ ), due to the push-pull nature of the donating hydroxyl and the withdrawing electron deficient heteroaromatic, the peak at 299 nm with a shoulder at 310 nm, a new band developed at 320 nm, and the absorption band at 360 nm also decreased and red shift, while a new band developed at 465 nm (Fig. 4A). Both new bands were attributed to H-bonding between phenolic O-H. The colour of the sensor **2** solution changed from colorless to red brown, which could be observed by the naked eye (Fig. 4A, inset). Increasing the amounts of the  $\text{F}^-$ , the absorption band at 360 nm became weak and disappear gradually (Fig. 4B). The absorbance ratio ( $A_{465}/A_{360}$ ) showed clear sigmoid dependence on the  $\text{F}^-$  concentration (Fig. S12). This ratiometric absorbance change could be potentially useful for quantitative determination of  $\text{F}^-$ . When the addition of the amount of  $\text{F}^-$  ion was greater than 1 equiv. sensor **2**, the absorbance reached saturation. The stoichiometry of the interaction reveals that a 1:1 between sensor **2** and  $\text{F}^-$ , also supported by Job's plot data (Fig. 4B, inset). The association constant for sensor **2** with  $\text{F}^-$  was calculated to be  $5.4 \times 10^4\ \text{M}^{-1}$  (Fig. S13). The response of sensor **2** for anion and the effect of coexisting ions to  $\text{2-F}^-$  had shown that the other competition anions did not interfere with the detection of  $\text{F}^-$  (Fig. S14).

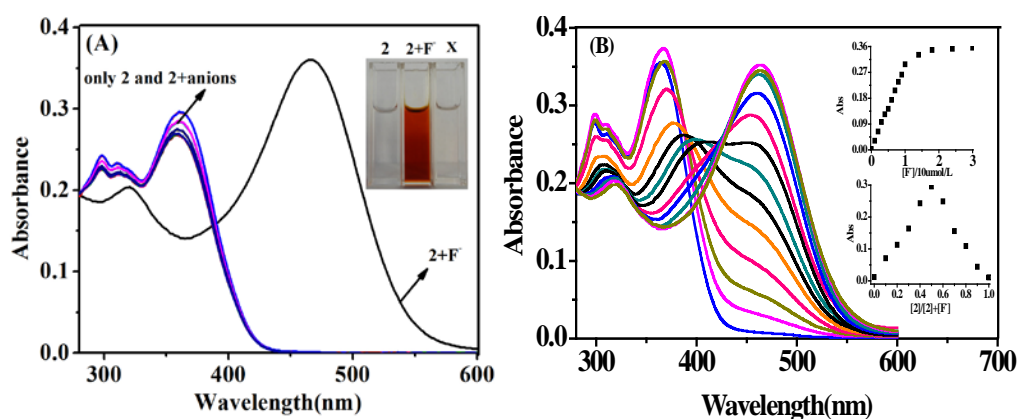


Fig. 4. Absorption spectra of sensor **2** ( $10\ \mu\text{M}$ ,  $\text{CH}_3\text{CN}$ ) with different anions (A), inset shows the color change of sensor **2** in the absence and the presence of  $\text{F}^-$  under visible light. Absorption spectra titrations of sensor **2** with  $\text{F}^-$  (B), inset shows variation of fluorescence intensity against the number of equivalents of  $\text{F}^-$  and Job's plot data. Anions ( $200\ \mu\text{M}$ ) include  $\text{F}^-$ ,  $\text{Cl}^-$ ,  $\text{Br}^-$ ,  $\text{I}^-$ ,  $\text{NO}_3^-$ ,  $\text{AcO}^-$ ,  $\text{H}_2\text{PO}_4^-$ ,  $\text{PF}_6^-$ ,  $\text{ClO}_4^-$ ,  $\text{HSO}_4^-$ .  $\lambda_{\text{max}} = 465\ \text{nm}$

### 3.2 The complex characteristics of sensor **2** with $\text{Al}^{3+}$ or $\text{F}^-$

### 3.2.1. Characteristics of isothermal titration calorimetry

Isothermal titration calorimetry (ITC) can provide complete thermodynamic parameters, including the binding enthalpy change ( $\Delta H$ ), entropy change ( $\Delta S$ ), binding constant ( $K$ ), and stoichiometry ( $n$ ) from a single titration, and offered the direct means of characterising the thermodynamic properties of molecules and molecules or ions interactions. The formation of the sensor **2** binding of  $\text{Al}^{3+}$  or  $\text{F}^-$  onto complexes was investigated by ITC in  $\text{CH}_3\text{CN}$  solution at 288.15 K. The sensor-ion titration is shown in Fig. 5A and 5B together with the integrated heats per mole of injectant (Fig. 5C, 5D). With the ion concentration increases, the bonding process were from the endothermic to exothermic then tend to saturated. The interaction of is mainly exothermic, but comprises a small endothermic contribution, and the thermodynamic parameters are listed in Table 1. Indicated the complexation of sensor **2** with  $\text{Al}^{3+}$  ( $\Delta H^\circ = -18.64 \pm 1.57 \text{ kJ}\cdot\text{mol}^{-1}$ ,  $T\Delta S^\circ = 15.496 \pm 0.36 \text{ kJ}\cdot\text{mol}^{-1}$ ) or with  $\text{F}^-$  ( $\Delta H^\circ = -55.83 \pm 2.34 \text{ kJ}\cdot\text{mol}^{-1}$ ,  $T\Delta S^\circ = 23.319 \pm 0.27 \text{ kJ}\cdot\text{mol}^{-1}$ ) are driven by both enthalpy and entropy. The value of  $\Delta G^\circ$  ( $\Delta G = \Delta H - T\Delta S$ ) are less than zero indicate that the binding process are spontaneous. The stoichiometrie of sensor bound to ion was about 1, respectively, and the binding constant ( $K$ ) of up to  $10^4 \text{ M}^{-1}$ . The experimental results of ITC are consistent with that of fluorescence and UV/vis spectra.

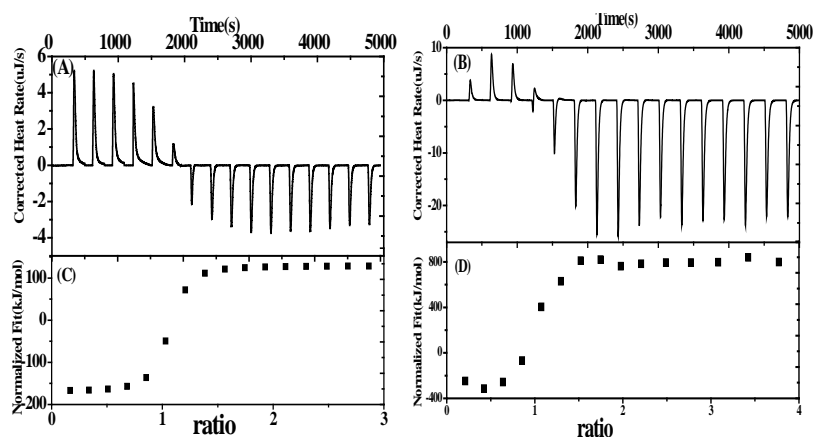


Fig. 5. ITC profile for the binding of sensor **2** ( $5 \times 10^{-5} \text{ M}$ ) to metal ions ( $1 \times 10^{-3} \text{ M}$ ) and its non-linear curve fitting.  $\text{Al}^{3+}$ : A, C;  $\text{F}^-$ : B, D

Table 1 Complex stability constant ( $K_a$ ), enthalpy ( $H^\circ$ ), and entropy change ( $T\Delta S^\circ$ ) for the complexation of sensor **2** with  $\text{Al}^{3+}$  or  $\text{F}^-$  in  $\text{CH}_3\text{CN}$  solution at 288.15 K

Complex	$n$	$K_a \text{ M}^{-1}$	$\Delta H^\circ \text{ kJ}\cdot\text{mol}^{-1}$	$T\Delta S^\circ \text{ kJ}\cdot\text{mol}^{-1}$
Sensor <b>2</b> +Al <sup>3+</sup>	0.986±0.024	5.62±0.042×10 <sup>4</sup>	-18.64±1.57	15.496±0.36
Sensor <b>2</b> + F <sup>-</sup>	0.967±0.018	8.02±0.012×10 <sup>4</sup>	-55.83±2.34	23.319±0.27

### 3.2.2. <sup>1</sup>H NMR titration of sensor **2** with Al<sup>3+</sup> or F<sup>-</sup>

<sup>1</sup>H NMR titration of sensor **2** with Al<sup>3+</sup> was examined in CD<sub>3</sub>CN in Fig. 6. It should be noted that the <sup>1</sup>H NMR spectrum of sensor **2** contains no signals for the OH proton due to a fast exchange with the solvent. Addition of 1.0 equiv. of Al(ClO<sub>4</sub>)<sub>3</sub> leads to the appearance of the chemical shifts signal of the phenolic hydroxyl (-OH) protons at about 12.85 ppm, 10.18 ppm, and 8.92 ppm. All the protons of quinoline and benzene ring downfield sifted from 0.01 ppm to 0.55 ppm, respectively. Due to the reduction of electron density upon lone pair of hydroxyl oxygen and the nitrogen atom of quinoline ring chelated with Al<sup>3+</sup> ion. <sup>1</sup>H NMR data demonstrated that the phenolic hydroxyl oxygen atom and nitrogen atom of quinoline is the binding site. After sensor **2** chelated with Al<sup>3+</sup>, all the protons of quinoline and benzene ring downfield sifted, indicated that with the effective binding of Al<sup>3+</sup> to the hydroxyl and nitrogen donor groups disruption of the internal charge transfer (ICT) [32-33] from the donor hydroxyl group to the acceptor quinoline moiety, it hence reducing the electron density around aromatic protons lead to signal downfield sifted.

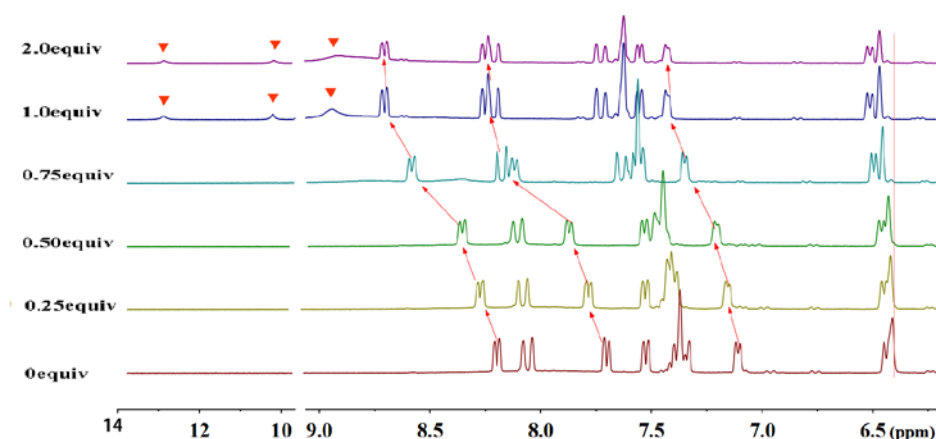


Fig. 6. The <sup>1</sup>H NMR in the absence and presence of Al<sup>3+</sup> for sensor **2**

To explore the sensing mechanism of sensor **2** to F<sup>-</sup>, the <sup>1</sup>H NMR titration in DMSO-*d*<sub>6</sub> were investigated, which illustrated the characteristic structural changes

occurring upon interaction with  $F^-$ . As shown in Fig.7, before the addition of  $F^-$ , the  $^1H$  NMR chemical shifts of the phenolic hydroxyl (-OH) protons were at  $\delta$  9.899 ppm, 9.642 ppm and 9.448 ppm respectively. Upon the gradual addition of  $F^-$ , the signal of -OH slightly downfield shift and broaden, this is attributed to the sensor **2** formed double hydrogen bonds between  $F^-$  and -OH group, after the presence of 1 equiv.  $F^-$ , all peaks of -OH gradually disappeared which indicating the formation of H-bonding between phenolic -OH and  $F^-$  (upon addition of excess amount of  $F^-$ , didn't observation of the H-O bond cleavage signals). Meanwhile, due to the formation of H-bonding, the protons of quinoline upfield shifted strengthen the polarity and electron-donating ability of -OH group, increase in the rigidity of planarity of sensor **2**, restricted the intramolecular rotation of sensor **2**, hence enhance the effective intramolecular charge transfer (ICT) induced by the electron push-pull system. The effect would explain the larger red-shift observed.

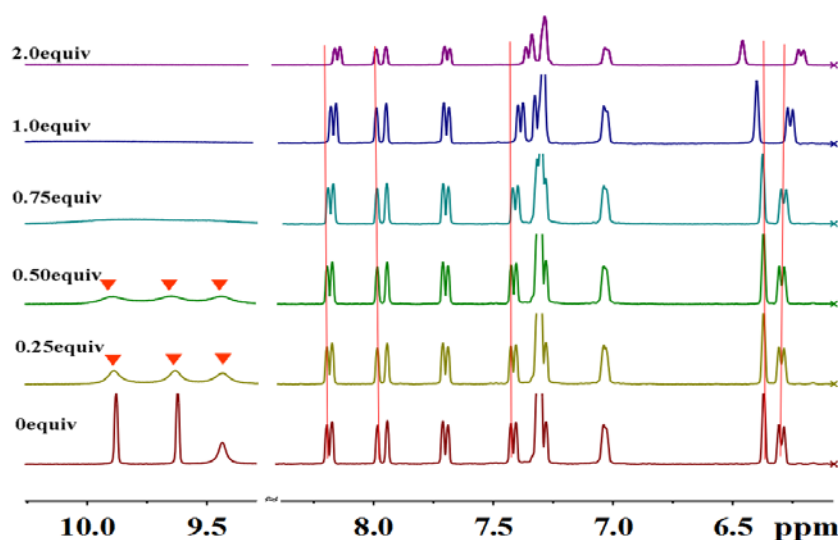


Fig. 7. The  $^1H$  NMR in the absence and presence of  $F^-$  for sensor **2**

### 3.2.3. The recognition mechanisms of sensor **2**

To confirm the stoichiometry between sensor **2** and  $Al^{3+}$  ion, ESI-MS examination was conducted (Fig. S15). Mass peaks at  $m/z$  309.0 and 280.0 corresponding to  $[2+Al-3H]^+$  and  $[2+H]^+$  are clearly observed, which gave evidence for the formation of a 1:1 complex, and the result are consistent with the spectral data. The IR spectra of the sensor **2**, **2**- $Al^{3+}$  and **2**- $F^-$  mixtures were also measured in the  $CH_3CN$  medium, respectively (Fig. S16). IR peak shifts have also been observed that the phenyl peak of

sensor **2** (1510, 1445  $\text{cm}^{-1}$ ) changed by adding either  $\text{Al}^{3+}$  or  $\text{F}^-$ ; indicated the participation of the hydroxyl on the phenyl in the complexation of sensor with ion. Combine with the  $^1\text{H}$  NMR, MS and IR results, the recognition mechanism of sensor **2** for  $\text{Al}^{3+}$  and  $\text{F}^-$  can be obtained.

### 3.2.4 Molecular switching behaviour of sensor **2**

Therefore, we further investigated the fluorescence characteristics of complex **2**- $\text{Al}^{3+}$  ( $10\ \mu\text{M}$ ,  $2:\text{Al}^{3+} = 1:1$ ) to various anions in the  $\text{CH}_3\text{CN}$ . As shown in Fig. 8A,  $\text{Cl}^-$ ,  $\text{Br}^-$ ,  $\text{I}^-$ ,  $\text{NO}_3^-$ ,  $\text{AcO}^-$ ,  $\text{H}_2\text{PO}_4^-$ ,  $\text{PF}_6^-$ ,  $\text{ClO}_4^-$ ,  $\text{HSO}_4^-$  give poor responses, while only  $\text{F}^-$  generates a significant fluorescence response. Addition of  $\text{F}^-$  to complex **2**- $\text{Al}^{3+}$  resulted in an obviously fluorescence quenching at 540 nm, showing the “on-off” fluorescence emission, and the fluorescence intensity decreases linearly related to the concentration of  $\text{F}^-$  (Fig. 8B). When 4 equiv. of  $\text{F}^-$  was added, sensor **2** reacted with  $\text{F}^-$ , the fluorescence enhanced at 563 nm, showing the “off-on” fluorescence emission (Fig. 8C). Sensor **2** behaves as a reversible “off-on” switch at 540 nm and 563 nm with  $\text{Al}^{3+}$  and  $\text{F}^-$  ions alternately (Fig. 8D).

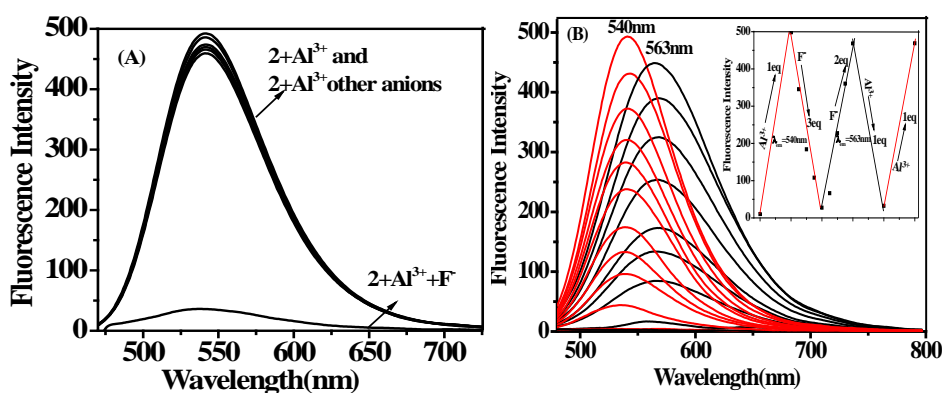


Fig. 8. (A) Fluorescence spectra of complex **2**- $\text{Al}^{3+}$  ( $10\ \mu\text{M}$ ) with different anions ( $30\ \mu\text{M}$ ),  $\lambda_{\text{ex}}/\lambda_{\text{em}} = 440/540\ \text{nm}$ ; (B) fluorescence spectra titrations of sensor **2** with the amounts of  $\text{Al}^{3+}$  and  $\text{F}^-$  alternately,  $\lambda_{\text{ex}}/\lambda_{\text{em}} = 440/540\ \text{nm}$ ,  $\lambda_{\text{ex}}/\lambda_{\text{em}} = 465/563\ \text{nm}$ . Inset shows the change of fluorescence intensity of sensor **2** with the amounts of  $\text{F}^-$  and  $\text{Al}^{3+}$  alternately. All experiments were carried out in  $\text{CH}_3\text{CN}$  with sensor **2** ( $10\ \mu\text{M}$ ). Anions include  $\text{F}^-$ ,  $\text{Cl}^-$ ,  $\text{Br}^-$ ,  $\text{I}^-$ ,  $\text{NO}_3^-$ ,  $\text{AcO}^-$ ,  $\text{H}_2\text{PO}_4^-$ ,  $\text{PF}_6^-$ ,  $\text{ClO}_4^-$ ,  $\text{HSO}_4^-$ .

To illustration of the optical switching process,  $^1\text{H}$  NMR spectra (Fig. 9) of the **2**, **2**+ $\text{F}^-$  and **2**+ $\text{F}^-$ + $\text{Al}^{3+}$  mixtures were measured. When 3 equiv. of  $\text{F}^-$  was added in sensor

**2**, the chemical shift signal of phenolic hydroxyl (-OH) protons at 9.90 ppm, 9.62 ppm and 9.44 ppm disappeared, this is attribute to the sensor **2** formed double hydrogen bonds between F<sup>-</sup> and -OH group. After addition of 1 equiv. Al<sup>3+</sup> to above mentioned 2-F<sup>-</sup> mixture, a significant chemical shift change of -OH protons appeared at 10.00 ppm, 9.91 ppm and 9.73 ppm were observed, the protons on the benzene shifted from 6.53 ppm to 6.39 ppm, and the protons on quinoline from 8.16 ppm to 8.19 ppm, respectively. All these indicated the occurrence of a competition reaction between Al<sup>3+</sup> and sensor **2** with F<sup>-</sup>, and then formed AlF<sub>3</sub> complex. Continue adding of 2 equiv. Al<sup>3+</sup>, the protons on quinoline shifted downfield from 8.19 ppm to 8.31 ppm, due to the reduction of electron density upon lone pair of hydroxyl oxygen, demonstrated the nitrogen atom of quinoline ring chelated with Al<sup>3+</sup> ion. These results proved the reversible “off-on” optical switch mode of sensor **2** with Al<sup>3+</sup> and F<sup>-</sup>, as shown in Scheme 2.

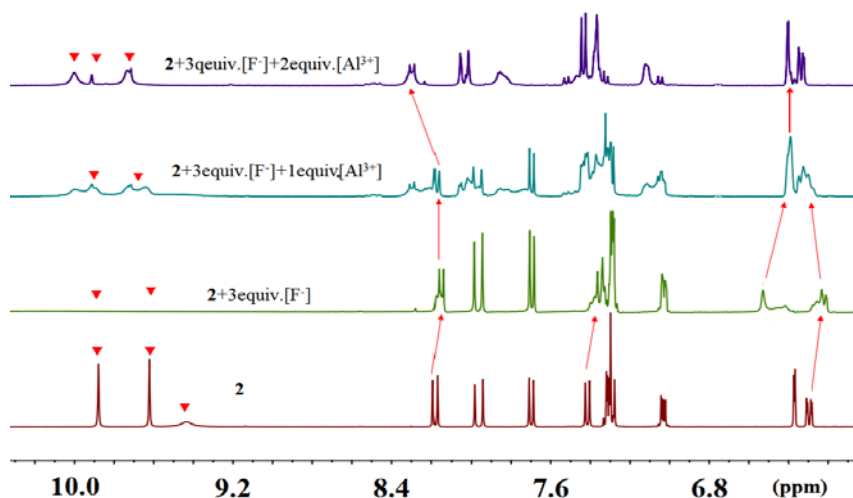


Fig. 9. The <sup>1</sup>H NMR in the absence and presence of F<sup>-</sup> and F<sup>-</sup>+Al<sup>3+</sup> for sensor **2**



Scheme 2. Graphic of the proposed mechanism of the sensing of Al<sup>3+</sup> and F<sup>-</sup>

### 3.3 Analysis Properties of sensor **2**

According to the above spectral behavior of sensor **2** for Al<sup>3+</sup>, the calibration curve

for the determination of  $\text{Al}^{3+}$  was constructed under the optimum conditions: sensor **2** ( $1.00 \times 10^{-5}$  M) in  $\text{CH}_3\text{CN}/\text{H}_2\text{O}$  solution (5/2, v/v, Tris-HCl buffer, pH 7,  $\lambda_{\text{ex}}/\lambda_{\text{em}} = 440/545$  nm). The fluorescence increment showed a linear relationship with the concentration of  $\text{Al}^{3+}$  in the range of  $6.0 \times 10^{-7} \sim 1.2 \times 10^{-5}$  M ( $R = 0.9937$ ,  $n = 10$ ). The absorbance measures at 430 nm were linearly related to the concentration of  $\text{Al}^{3+}$  in the range of  $8.0 \times 10^{-7} \sim 1.2 \times 10^{-5}$  M ( $R = 0.9974$ ,  $n = 10$ ). The limit of detection based on 10 blank determinations was  $0.06 \mu\text{M}$  (fluorescence measurement) and  $0.32 \mu\text{M}$  (UV-vis measurement) respectively (Fig. S17). Under the same conditions, the determination of  $\text{Al}^{3+}$  in a synthetic sample solution was carried out using the proposed fluorescence and absorption method. The results are listed in Table S1, which shows satisfactory recovery and R.S.D. values for the sample.

#### 4. Conclusion

A simple structure quinaldine derivative was synthesized facilely, not only exhibited as an “off-on” fluorescence/colorimetric sensor for  $\text{Al}^{3+}$  but also for  $\text{F}^-$  ion. The sensor shown facilitates “naked-eye” detection, remarkably specific discrimination  $\text{Al}^{3+}$  or  $\text{F}^-$  from other competition ions with intrinsic large Stoke’s shift. The identification was proved to the ICT mechanism by  $^1\text{H}$  NMR, UV-vis, ITC and fluorescence spectrum. The sensor behaves as a reversible “off-on” and “on-off” switch by sequential inputs two ions of  $\text{Al}^{3+}$  and  $\text{F}^-$  ions, constituted a very favorable optical switch-mode.

#### Acknowledgement

We are grateful for the financial support from the Natural Science Foundation of China (No. 21165006), the Fund of the International Cooperation Projects of Guizhou Province (No. 20137002), “Chun-Hui” Fund of Chinese Ministry of Education (No. Z2011033, Z2012053) and Major Scientific Equipment Developed Special Project of China (2011YQ120035). The EPSRC is thanked for the financial support (Overseas Travel award to CR).

#### References

- [1] Que EL, Domaille DW, Chang CJ. Metals in Neurobiology: Probing Their Chemistry and Biology with Molecular Imaging. *Chem Rev* 2008; 108: 1517-1549.

- [2] Prodi L, Bolletta F, Montalti M, Zaccheroni N. Luminescent chemosensors for transition metal ions. *Coord Chem Rev* 2000; 205: 59-83.
- [3] Yang JL. Citrate transporters play a critical role in aluminium-stimulated citrate efflux in rice bean (*Vigna umbellata*) roots. *Ann Bot* 2006; 97: 579-584.
- [4] Kochian LV, Hoekenga OA. How do crop plants tolerate acid soils Mechanisms of aluminum tolerance and phosphorous efficiency. *Annu Rev Plant Biol* 2004; 55: 459-493.
- [5] Srinivasan P, Viraraghavan T, Subramanian K. Aluminium in drinking water: an overview. *Water SA* 1999; 25: 47-56.
- [6] Nayak P. Aluminum: impacts and disease. *Environ Res* 2002; 89: 101-115.
- [7] Walton JR, Aluminum in hippocampal neurons from humans with Alzheimer's disease. *Neuro Toxicol* 2006; 27: 385-394.
- [8] Kleerekoper M. The role of fluoride in the prevention of osteoporosis. *Endocrinology and Metabolism Clinics of North America* 1998; 27: 441-452.
- [9] Browne D, Whelton H, Mullane D. Fluoride metabolism and fluorosis. *Journal of Dentistry* 2005; 33: 177-186.
- [10] René P, Schwarzenbach, Escher BI, Fenner K, Hofstetter TB, Johnson CA, Gunten U, Wehrli B. The Challenge of micropollutants in aquatic systems. *Science* 2006; 313: 1072-1077.
- [11] Jagtap S, Yenkie MK, Labhsetwar N, Rayalu S. Fluoride in drinking water and defluoridation of water. *Chemical Reviews* 2012; 112: 2454-2466.
- [12] Silva AP, Gunaratne HQN, Gunnlaugsson T, Huxley AJM, McCoy CP, Rademacher JT, et al. Signaling recognition events with fluorescent sensors and switches. *Chem Rev* 1997; 97: 1515-1566.
- [13] Valeur B, Leray I. Design principles of fluorescent molecular. *Coord Chem Rev* 2000;205:3-40.
- [14] Bao YY, Liu B, Du FF, Tian J, Wang H, Ruke B. A new strategy for highly selective fluorescent sensing of F<sup>-</sup> and Zn<sup>2+</sup> with dual output modes. *J Mater Chem* 2012; 22: 5291-5294.
- [15] Hamid K, Khatereh R. Naked-eye detection of inorganic fluoride in aqueous media using a new azo-azomethine colorimetric receptor enhanced by electron withdrawing groups. *RSC Adv* 2014; 4: 1032-1038.
- [16] Sheri M, Mangalampalli R. Boron-Dipyrrromethene Based Reversible and Reusable Selective

Chemosensor for Fluoride Detection. *Inorg Chem* 2014; 53: 1646-1653.

[17] Punidha S, Lee CH. Highly Sensitive Fluorescence “Turn-On” Indicator for Fluoride Anion with Remarkable Selectivity in Organic and Aqueous Media. *J Org Chem* 2011; 76: 3820-3828.

[18] Sudipta D, Mili D, Debasis D. Fluorescent sensors for selective determination of trace level  $Al^{3+}$ : recent developments and future prospects. *Anal Methods* 2013; 5: 6262-6285.

[19] Soham S, Bhaskar N, Jubaraj BB. Hydrolytically stable Schiff base as highly sensitive aluminium sensor. *Inorganic Chemistry Communications* 2012; 22: 98-100.

[20] Subarna G, Sisir L, Animesh S, Arnab B, Damir AS, Maria GB, Mariusz PM, Michael B, Yann G, Subhra KM, Debasis D. A coumarin-based “turn-on” fluorescent sensor for the determination of  $Al^{3+}$ : single crystal X-ray structure and cell staining properties. *Dalton Trans* 2013; 42: 10198-10207.

[21] Noh JY, Kim S, Hwang IH, Lee GY, Kang J, Kim SH, Min J, Park S, Kim C, Kim J. Solvent-dependent selective fluorescence assay of aluminum and gallium ions using julolidine-based sensor. *Dyes and Pigments* 2013; 99: 1016-1021.

[22] Hou FP, Huang L, Xi PX, Cheng J, Zhao XF, Xie GQ, Shi YJ, Cheng FJ, Yao XJ, Bai DC, Zeng ZZ. A Retrievable and Highly Selective Fluorescent Sensor for Monitoring Sulfide and Imaging in Living Cells. *Inorg Chem* 2012; 51: 2454-2460.

[23] Fu Y, Mu L, Zeng X, Zhao JL, Redshaw C, Ni XL, Yamato T. An NBD-armed thiacalix[4]arene-derived colorimetric and fluorometric chemosensor for  $Ag^+$ : a metal–ligand receptor of anions. *Dalton Trans* 2013; 42: 3552-3560.

[24] Soroka K, Vithanage RS, Phillips DA, Walker B, Dasgupta PK. Fluorescence Properties of Metal Complexes of 8-Hydroxyquinoline-5-sulfonic Acid and Chromatographic Applications. *Anal Chem* 1987; 59: 629.

[25] Jiang X, Wang B, Yang Z. 8-Hydroxyquinoline-5-carbaldehyde Schiff-base as a highly selective and sensitive  $Al^{3+}$  sensor in weak acid aqueous medium. *Inorg Chem Commun* 2011; 14: 1224-1227.

[26] Zhang H, Han LF, Zachariasse KA, Jiang YB. 8-Hydroxyquinoline Benzoates as Highly Sensitive Fluorescent Chemosensors for Transition Metal Ions. *Org Lett* 2005; 19: 4217-4220.

[27] Song KC, Kim JS, Park SM, Chung KC, Ahn S, Chang SK. Fluorogenic  $Hg^{2+}$ -selective chemodosimeter derived from 8-Hydroxyquinoline. *Org Lett* 2006; 8: 3413-3416.

[28] Zhou XY, Li PX, Shi ZH, Tang XL, Chen CY, Liu WS. A highly selective fluorescent sensor for distinguishing cadmium from zinc ions based on a quinoline platform. *Inorg Chem* 2012; 51: 9226-9231.

[29] Zhou XY, Li PX, Shi ZH, Tang XL, Chen CY, Liu WS. A Highly Selective Fluorescent Sensor for Distinguishing Cadmium from Zinc Ions Based on a Quinoline Platform. *Inorg Chem* 2012; 51: 9226-9231.

[30] Ye WP, Wang SX, Meng XM, Feng Y, Sheng HT, Shao ZL, Zhu MZ, Guo QX. A novel Zn<sup>2+</sup> complex as the ratiometric two-photon fluorescent sensor for biological Cd<sup>2+</sup> detection. *Dyes and Pigments* 2014; 101: 30-37.

[31] Praveen L, Suresh CH, Reddy MLP, Varma RL. Molecular fluorescent sensor for Zn<sup>2+</sup> based on 2-(2-nitrostyryl)-8-methoxyquinoline. *Tetrahedron Letters* 2011; 52: 4730-4733.

[32] Shiraishi Y, Ichimura C, Sumiya S, Hirai T, Multicolor Fluorescence of a Styrylquinoline Dye Tuned by Metal Cations. *Chem. Eur* 2011; 17: 8324-8332.

[33] Ma Y, Chen HY, Wang F, Kamban S, Wang Y, Mao C, Chen XQ. A highly sensitive and selective ratiometric fluorescent sensor for Zn<sup>2+</sup> ion based on ICT and FRET. *Dyes and Pigments* 2014; 102: 301-307.

## Figure captions

### Scheme 1 Synthesis of quinaldine derivative **1** and sensor **2**

**Fig. 1.** Fluorescence spectra of sensor **2** (10  $\mu\text{M}$ , CH<sub>3</sub>CN/H<sub>2</sub>O, v/v, 5/2, pH 7) with different metal ions (A), inset shows the color change of sensor **2** in the absence and the presence of Al<sup>3+</sup> under UV light. The spectra titrations of sensor **2** with Al<sup>3+</sup> (B), inset shows variation of fluorescence intensity against the number of equivalents of Al<sup>3+</sup> and Job's plot data. Metal ions (200  $\mu\text{M}$ ) including Li<sup>+</sup>, Na<sup>+</sup>, K<sup>+</sup>, Mg<sup>2+</sup>, Ca<sup>2+</sup>, Ba<sup>2+</sup>, Sr<sup>2+</sup>, Hg<sup>2+</sup>, Pb<sup>2+</sup>, Cd<sup>2+</sup>, Zn<sup>2+</sup>, Co<sup>2+</sup>, Ni<sup>2+</sup>, Cu<sup>2+</sup>, Ag<sup>+</sup>, Cr<sup>3+</sup>, Fe<sup>3+</sup>.  $\lambda_{\text{ex}}/\lambda_{\text{em}} = 440/545 \text{ nm}$

**Fig. 2.** Absorption spectra of sensor **2** (10  $\mu\text{M}$ , CH<sub>3</sub>CN/H<sub>2</sub>O, 5/2, v/v, pH 7) with different metal ions (A), inset shows the color change of sensor **2** in the absence and the presence of Al<sup>3+</sup> under visible light. The spectra titrations of **2** with Al<sup>3+</sup> (B). Metal ions (200  $\mu\text{M}$ ) including Li<sup>+</sup>, Na<sup>+</sup>, K<sup>+</sup>, Mg<sup>2+</sup>, Ca<sup>2+</sup>, Ba<sup>2+</sup>, Sr<sup>2+</sup>, Hg<sup>2+</sup>, Pb<sup>2+</sup>, Cd<sup>2+</sup>, Zn<sup>2+</sup>, Co<sup>2+</sup>, Ni<sup>2+</sup>, Cu<sup>2+</sup>, Ag<sup>+</sup>, Cr<sup>3+</sup>, Fe<sup>3+</sup>.  $\lambda_{\text{max}} = 430 \text{ nm}$

**Fig. 3.** Fluorescence spectra of sensor **2** (10  $\mu\text{M}$ , CH<sub>3</sub>CN) with different anions (A), inset shows the color change of sensor **2** in the absence and the presence of F<sup>-</sup> under UV light. Fluorescence

spectra titrations of sensor **2** with F<sup>-</sup> (B), inset shows variation of fluorescence intensity against the number of equivalents of F<sup>-</sup> and Job's plot data. Anions (200 μM) include Cl<sup>-</sup>, Br<sup>-</sup>, I<sup>-</sup>, NO<sub>3</sub><sup>-</sup>, AcO<sup>-</sup>, H<sub>2</sub>PO<sub>4</sub><sup>-</sup>, PF<sub>6</sub><sup>-</sup>, ClO<sub>4</sub><sup>-</sup>, HSO<sub>4</sub><sup>-</sup>. λ<sub>ex</sub>/λ<sub>em</sub>=465/575 nm.

**Fig. 4.** Absorption spectra of sensor **2** (10 μM, CH<sub>3</sub>CN) with different anions (A), inset shows the color change of sensor **2** in the absence and the presence of F<sup>-</sup> under visible light. Absorption spectra titrations of sensor **2** with F<sup>-</sup> (B), inset shows variation of fluorescence intensity against the number of equivalents of F<sup>-</sup> and Job's plot data. Anions (200 μM) include F<sup>-</sup>, Cl<sup>-</sup>, Br<sup>-</sup>, I<sup>-</sup>, NO<sub>3</sub><sup>-</sup>, AcO<sup>-</sup>, H<sub>2</sub>PO<sub>4</sub><sup>-</sup>, PF<sub>6</sub><sup>-</sup>, ClO<sub>4</sub><sup>-</sup>, HSO<sub>4</sub><sup>-</sup>. λ<sub>max</sub> = 465 nm

**Fig. 5.** ITC profile for the binding of sensor **2** (5×10<sup>-5</sup> M) to metal ions (1×10<sup>-3</sup> M) and its non-linear curve fitting. Al<sup>3+</sup>: A, C; F<sup>-</sup>: B, D

**Fig. 6.** The <sup>1</sup>H NMR in the absence and presence of Al<sup>3+</sup> for sensor **2**

**Fig. 7.** The <sup>1</sup>H NMR in the absence and presence of F<sup>-</sup> for sensor **2**

**Fig. 8.** Fluorescence spectra of complex **2**-Al<sup>3+</sup> (10 μM) with different anions (30 μM).

(A), λ<sub>ex</sub>/λ<sub>em</sub>=440/540 nm. Fluorescence spectra titrations of complex **2**-Al<sup>3+</sup> with F<sup>-</sup> (B), λ<sub>ex</sub>/λ<sub>em</sub>=440/540 nm, (C) λ<sub>ex</sub>/λ<sub>em</sub>=465/563 nm. Change of fluorescence intensity of complex **2**+Al<sup>3+</sup> with the amounts of F<sup>-</sup> and Al<sup>3+</sup> (D). 1-2: the emission intensity of addition of Al<sup>3+</sup> (10 μM), 2-3: the emission intensity of addition of F<sup>-</sup> (50 μM). 3-4: the emission intensity of addition of Al<sup>3+</sup> (10 μM). All experiments were carried out in CH<sub>3</sub>CN with sensor **2** (10 μM). Anions include F<sup>-</sup>, Cl<sup>-</sup>, Br<sup>-</sup>, I<sup>-</sup>, NO<sub>3</sub><sup>-</sup>, AcO<sup>-</sup>, H<sub>2</sub>PO<sub>4</sub><sup>-</sup>, PF<sub>6</sub><sup>-</sup>, ClO<sub>4</sub><sup>-</sup>, HSO<sub>4</sub><sup>-</sup>.

**Fig. 9.** The <sup>1</sup>H NMR in the absence and presence of F<sup>-</sup> and F<sup>-</sup>+Al<sup>3+</sup> for sensor **2**

**Scheme 2.** Graphic of the proposed mechanism of the sensing of Al<sup>3+</sup> and F<sup>-</sup>